Transmission through array of subwavelength metallic slits curved with a single step or multi-step*

Wang Ying-Qi(王瑛琪)[a)b)†], Wang Yan-Hua(王艳花)[c)], Zheng Xian-Hua(郑显华)[b)], Ye Jia-Sheng(叶佳声)[b)], Zhang Yan(张 岩)[a)b)‡], and Liu Shu-Tian(刘树田)[a)]

[a)] *Department of Physics, Harbin Institute of Technology, Harbin* 150001, *China*
[b)] *Department of Physics, Capital Normal University, Beijing* 100048, *China*
[c)] *Institute of Microelectronics of Chinese Academy of Sciences, Beijing* 100029, *China*

(Received 17 April 2013; revised manuscript received 1 August 2013; published online 14 January 2014)

The transmission of normally incident plane wave through an array of subwavelength metallic slits curved with a single step or multi-step has been explored theoretically. The transmission spectrum is simulated by using the finite-difference time-domain method. The influences of surface plasmon polaritons make the end of finite long sub-wavelength metallic slit behaves as magnetic-reflecting barrier. The electromagnetic fields in the subwavelength metallic slits are the superposition of standing wave and traveling wave. The standing electromagnetic oscillation behaves like LC oscillating circuit to decide the resonance wavelength. Therefore, the parameters of adding step may change the LC circuit and influence the transmission wavelength. A new explanation model is proposed in which the resonant wavelength is decided by four factors: the changed length for electric field, the changed length for magnetic field, the effective coefficient of capacitance, and the effective coefficient of inductance. The effect of adding step is presented to analyze the interaction of two steps in slit with multi-step. This explanation model has been proved by the transmission through arrayed subwavelength metallic slits curved with two steps and fractal steps. All calculated results are well explained by our proposed model.

Keywords: surface plasmon polaritons, metal optics

PACS: 42.25.Bs, 78.20.Bh **DOI:** 10.1088/1674-1056/23/3/034202

1. Introduction

Since Ebbesen *et al* discovered the extraordinary optical transmission (EOT) through a sub-wavelength hole array in an optically thin metallic film,[1] enhanced transmission through sub-wavelength metallic structures has attracted great interest [2–5]. Besides sub-wavelength hole arrays,[6–10] the researches of only one slit and slit arrays,[11–20] such as the basic functions of EOT, are topics of considerable fascination in achieving high transmission in several applications,[21–23] including superlenses and optical filters.

The initial work owes the EOT to surface plasmon polaritons (SPPs), which propagate along the interface between the metallic film and dielectric, and are modulated by slits or apertures in optical, infrared, terahertz and microwave regions. From Maxwell's equations, the SPP mode must be a transverse magnetic mode. In a metallic slit structure the propagating TM modes can be supported without cutoff. For an optically metallic thin plate, the high transmission of slits is due to the SPP intensification and the Fabry–Perot (F–P) interference. Up to now, most researchers put their emphasis on the surface structure of the metal plate to modulate SPPs. However, the dependence of transmission on the conformation inside apertures is not fully investigated.

As the nanotechnology develops, the experimental investigation on the conformation inside metal apertures is possible. Lockyear *et al* investigated the transmission of a normally incident plane wave through a singly stepped sub-wavelength slit in the microwave region [24]. The existence of the step, which is located in the middle of the slits, increases the resonant wavelength substantially. The field at resonant frequencies shows that the transmission maximum corresponds to the fundamental F–P mode. Recently, we theoretically studied the transmission spectra of periodic slits modified by the perpendicular cuts in a metal plate in the near infrared region [25]. The existence of cuts in the middle of slits decreases the resonant wavelength of the even-order F–P mode, which is quite different from the case of the odd-order mode. The parameters of cuts, including the location and width, change the resonant wavelength complexly. In the following work, we found that the added corner between the slit and waveguide can also affect the resonant wavelength [26]. The symmetric electromagnetic field distributed in the waveguide is decided by the length of waveguide, which makes the location of the waveguide change the resonant wavelength. The antisymmetric electromagnetic field distribution is also decided by the length of waveguide, which makes that the location does not change the resonant wavelength.

*Project supported by the National Basic Research Program of China (Grant No. 2011CB301801), the National Natural Science Foundation of China (Grant Nos. 10904099, 11174211, 11204188, and 61205097), and the Natural Science Foundation of Beijing, China (Grant No. KZ201110028035).

†Corresponding author. E-mail: wangyingqi.hit@gmail.com
‡Corresponding author. E-mail: yzhang@mail.cnu.edu.cn

© 2014 Chinese Physical Society and IOP Publishing Ltd

From all the above research, it was found that the field in the slit is the main factor in deciding the transmission wavelength. The structure inside the slit can easily influence the field in the slit. Therefore, in this paper, for investigating the influence of the conformation inside the apertures, we study the transmission of the normally incident plane wave through an array of sub-wavelength metallic slits curved with a single step or multi-step, theoretically.

This article is arranged as follows: Section 2 describes the structure under investigation and the dispersion equation of the metal. Section 3 presents the theoretical mode of the resonant wavelength and the calculated transmission spectra by using the finite-difference time-domain (FDTD) method. Finally, a conclusion is drawn in Section 4.

2. Metallic structures and numerical tools

A schematic of a unit cell of the one-dimensional metallic grating is shown in Fig. 1. The parameters are denoted by the period of the slits p, the thickness of the metallic film h_1, and the width w_1 of the grating slit. The parameters of the modified step are width w_2, length h_2, and vertical position h_3, as shown in Fig. 1. In this work, the influence of adding single or multi-steps on transmission is investigated.

Two-dimensional EM fields inside and near the metallic film are simulated by the FDTD [27,28] method. The calculated region is truncated by the perfectly matched layers on the top and bottom boundaries. The left and right boundaries are treated as periodic boundary conditions due to the periodicity of the structure. The incident light is along the z direction with TM polarization, (i.e., the incident electric field E_0 is along the x direction). When a pulsed plane wave is incident upon the periodic metal structure, the time-domain field $E(t)$ is recorded on the output plane. Then, the frequency spectrum $E(\omega)$ can be easily achieved via the Fourier transform method.

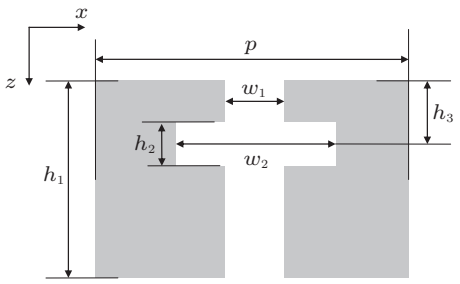


Fig. 1. Schematic of a unit cell of the periodic metallic slit with perpendicular step.

Since the dielectric response of the metal is mainly governed by its free electron plasmon, the frequency-dependent permittivity of the metal is expressed by the Drude model as

$$\varepsilon(\omega) = 1 - \frac{\omega_p^2}{\omega(\omega + i\gamma)}, \tag{1}$$

where ω_p is the plasma frequency, γ is the absorption coefficient, and ω is the frequency. The metal investigated is silver and the considered wavelength range is from 800 nm to 1800 nm. The corresponding parameters are $\omega_p = 1.37 \times 10^{16}$ rad/s and $\gamma = 3.21 \times 10^{13}$ rad/s [29]. When $\omega < \omega_p$, the real part of the permittivity is negative, the standard time iteration scheme of the FDTD method becomes unstable. However, this problem can be solved by introducing the current density[30,31] into Maxwell's equations.

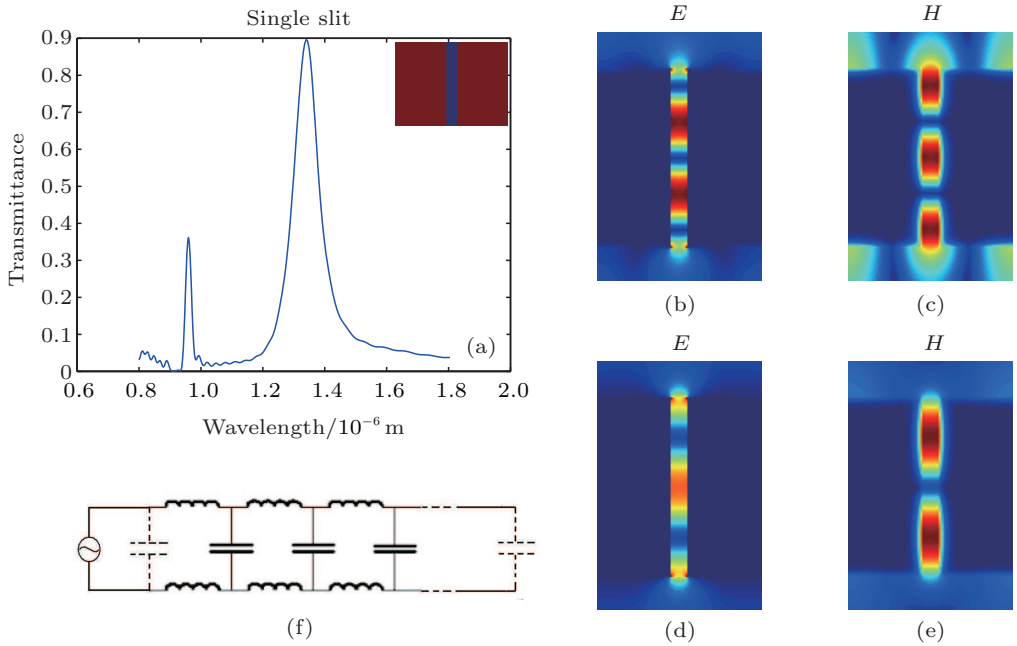


Fig. 2. (color online) The transmission spectra of single slit (a), the electric field (b) of the first transmission peak in panel (a), the magnetic field (c) of the first transmission peak, the electric field (d) of the second transmission peak, the magnetic field (e) of the second transmission peak, and the equivalent circuits diagram (f) of the slit.

For an array of slits without a step, the parameters are chosen as $p = 900$ nm, $h_1 = 972$ nm, and $w_1 = 90$ nm. The thickness of the metallic film is prepared for the fractal structure. Two resonant wavelengths (956 nm and 1340 nm) are obtained in the considered wavelength range by using the FDTD method. Obviously, the slits act as the F–P cavities according to Ref. [32], and the mode number is $N = 3$ for $\lambda = 956$ nm and $N = 2$ for $\lambda = 1340$ nm. Figure 2(a) presents the transmission spectra of the slit without any steps. Figure 2(b) describes the electric field in the slit for the first transmission peak in Fig. 2(a), figure 2(c) is the magnetic field for the first transmission peak, figure 2(d) is the electric field for the second transmission peak, figure 2(e) is the magnetic field for the second transmission peak, and figure 2(f) presents the equivalent circuit diagram of the standing oscillation.

3. Theoretical mode and calculated results

3.1. Electromagnetic field in an array of slits

In the infinite sub-wavelength metallic slit, the electromagnetic field can be represented by a TM waveguide mode

$$\begin{aligned} E(x,y,t) &= E_0\left[\exp(-\mathrm{i}k_x x)+\exp(\mathrm{i}k_x x)\right] \\ &\quad\times \exp(\mathrm{i}k_{\mathrm{w}} y-\mathrm{i}\omega t), \end{aligned} \tag{2}$$

$$\begin{aligned} H(x,y,t) &= H_0\left[\exp(-\mathrm{i}k_x x)+\exp(\mathrm{i}k_x x)\right] \\ &\quad\times \exp(\mathrm{i}k_{\mathrm{w}} y-\mathrm{i}\omega t+\pi/2). \end{aligned} \tag{3}$$

In Eqs. (2) and (3), the x direction wave vector is represented by $k_x = (k_0^2\varepsilon_{\mathrm{d}} - k_{\mathrm{w}}^2)^{1/2}$. The propagation constant of the metallic slit waveguide k_{w} is a solution of transcendental equation $k_x d = m\pi + 2\arctan[\varepsilon_{\mathrm{d}}\left(k_{\mathrm{w}}^2 - k_0^2\varepsilon_{\mathrm{m}}\right)^{1/2}/\varepsilon_{\mathrm{m}}k_x]$, ε_{m} and ε_{d} are the metal permittivity and the dielectric permittivity, respectively, m is the waveguide mode number, $\pi/2$ is the phase difference between the electric and magnetic field. When the width of the waveguide is far less than the incident wavelength, only a basic electromagnetic field exists.

For the case of a finite sub-wavelength metallic slit, charge accumulation exists at the corners between the metallic surface and slit. Electric field near the corner keeps very strong, correspondingly. Magnetic field is approximately zero because surface current is also approximately zero at the corner. Therefore, the end of the slit can be represented by a magnetic-reflecting barrier, unlike the reflecting mirror in Fabry–Perot etalon which acts as an electric-reflecting barrier.

At a microscopic level, the electromagnetic field in the slit looks like F–P interference. However, from waveguide theory, the difference of reflectivity between the air in slit and the outside air is very small, the Q factor of the cavity can not support the wide spectrum. Liu *et al* owed this phenomenon to the scatters of the SPP and quasi-cylindrical wave (CW) [33]. They also pointed out that the CW contribution is merely dependent of metal dielectric, whereas the SPP contribution rapidly drops with the increase of the metal conductivity. In this paper, the CW contribution and the reflectivity of waveguide mode are owed to basic reflectivity. The reflectivity and the transmittance coefficients t_A and r_A (where A refers to all) for normal incidence represent as

$$r_A = r + \frac{2\alpha^2}{u^{-1} - (\rho+\tau)}, \tag{4}$$

$$t_A = t + \frac{2\alpha\beta}{u^{-1} - (\rho+\tau)}, \tag{5}$$

where r and t denote reflectivity and transmittance coefficients of the CW contribution and the waveguide mode, α is the scattering coefficient from the SPP mode to the waveguide mode, β is the scattering coefficient from the SPP mode to the outgoing plane wave, ρ is the reflectance coefficient of the SPP mode via the slit along the metallic interface, and τ is the transmittance coefficient of the SPP mode, $u = \exp(\mathrm{i}k_{\mathrm{SPP}}p)$ is the phase delay accumulated by the SPP over a grating period,

$$k_{\mathrm{SPP}} = k_0\sqrt{\frac{\varepsilon_{\mathrm{m}}\varepsilon_{\mathrm{d}}}{\varepsilon_{\mathrm{m}}+\varepsilon_{\mathrm{d}}}}$$

is the complex propagation constant of a SPP on the flat metal-dielectric interface; ε_{m} and ε_{d} are the metal permittivity and the dielectric permittivity, respectively; k_0 is the propagation constant of light in the air.

Because of the magnetic-reflecting barrier, there are forward and backward waves in the slits. The field in the slits can be represented by

$$\begin{aligned} E &= 2E_{\mathrm{i}}r_A\cos(k_{\mathrm{w}}y)\exp(-\mathrm{i}\omega t) \\ &\quad+(1-r_A)E_{\mathrm{i}}\exp(\mathrm{i}k_{\mathrm{w}}y-\mathrm{i}\omega t), \end{aligned} \tag{6}$$

$$\begin{aligned} H &= 2H_{\mathrm{i}}r_A\cos(k_{\mathrm{w}}y+\pi/2)\exp(-\mathrm{i}\omega t) \\ &\quad+(1-r_A)H_{\mathrm{i}}\exp(\mathrm{i}k_{\mathrm{w}}y-\mathrm{i}\omega t+\pi/2). \end{aligned} \tag{7}$$

In Eqs. (6) and (7), r_A is the total reflectivity coefficient, which can be calculated from Eq. (4), E_{i} (H_{i}) represents the electric (magnetic) field independent of the z coordinate. The former signifies the standing wave field and the latter signifies the traveling wave field. The standing wave decides the peak wavelength of transmittance while the traveling wave mainly carries the transmitted energy.

In a sub-wavelength metallic slit, the surface electromagnetic wave is transmitted by surface charge and surface current. The surface charge density and current density are derived by the field near the metallic surface

$$\begin{aligned} \sigma &= \boldsymbol{n}\cdot\boldsymbol{D} \\ &= \varepsilon_{\mathrm{d}}E_{\mathrm{i}}\left[2r_A\cos\left(k_{\mathrm{w}}y\right)+\left(1-r_A\right)\exp\left(\mathrm{i}k_{\mathrm{w}}y\right)\right] \\ &\quad\times\exp\left(-\mathrm{i}\omega t\right), \end{aligned} \tag{8}$$

$$\begin{aligned} \boldsymbol{j} &= \boldsymbol{n}\times\boldsymbol{H} \\ &= H_{\mathrm{i}}\left[2r_A\cos\left(k_{\mathrm{w}}y+\pi/2\right)+\left(1-r_A\right)\exp\left(\mathrm{i}k_{\mathrm{w}}y+\pi/2\right)\right] \\ &\quad\times\exp\left(-\mathrm{i}\omega t\right), \end{aligned} \tag{9}$$

where $\boldsymbol{n}$ is a unit normal vector directed from metal into air in the slit, $\boldsymbol{H}$ and $\boldsymbol{D}$ are magnetic field and electric displacement, $\boldsymbol{j}$ and σ are surface current density and surface charge density.

As the electric (or magnetic) field can be represented by the superposition of the standing wave and traveling wave in the slit, the surface charge density σ (or the surface current density $\boldsymbol{j}$) can also be represented by the superposition of the standing oscillation and traveling oscillation. The standing electromagnetic oscillation behaves like an LC oscillating circuit to select resonance frequency. While the traveling wave has the function to transmit light energy. Because r_A is close to one in the metallic grating, the electromagnetic field in the slit is mainly a standing wave. Corresponding to this case, the charge oscillation at the metallic wall is also mainly a standing wave. As the charge accumulates at the corners of the upper and lower ends of the slit, the upper and lower ends of the slit must be represented by the imaginary capacitance. As the phase difference between charge density and current, the current locates at $\lambda_{\rm w}/4$ away from the place where the charge is accumulated, $\lambda_{\rm w} = 2\pi/k_{\rm w}$ is the effective wavelength of the waveguide mode. Therefore, the equivalent circuit diagram can be represented by the alternation of inductance and capacitance.

3.2. Transmission of slits with a single-step

If the mode volume of an additional step is smaller than the incident light, this structure can be considered as the perturbation of optical field already formed in the slit. In this case, the additional step can only affect one period of the equivalent circuit diagram. The location of the step affects the values of equivalent inductance and capacitance. For analyzing the influence of location and geometric dimension of the additional step, we introduce the relative coefficient of capacitance $\eta_{\rm C}$ and the relative coefficient of inductance $\eta_{\rm L}$ as

$$\eta_{\rm C} = \int_{\rm step} \sigma \,{\rm d}y \Big/ \int_{\rm period} \sigma \,{\rm d}y, \tag{10}$$

$$\eta_{\rm L} = \int_{\rm step} j \,{\rm d}y \Big/ \int_{\rm period} j \,{\rm d}y, \tag{11}$$

where the integral subscript 'step' and 'period' represent the step's location and one period of the equivalent diagram, respectively.

As the $\pi/2$ phase difference between charge density and current density, when the relative coefficient of capacitance $\eta_{\rm C}$ achieves maximum, the relative coefficient of inductance $\eta_{\rm L}$ must reach a minimum. In this case, the slit can be considered as a parallel-plate capacitor and the step mainly influences the accumulating charge. The charge on one of the metallic slit walls must be opposite to that on the other. The corner between step and slit would accumulate charge. The charge has the same sign on the same side of slit. For the traveling wave, it looks like electromagnetic field transmits directly across the step. From this point of view, the influence of the step is equivalent to shortening the length of the slit. The decrement is denoted by δQ. When the effective coefficient of the inductance $\eta_{\rm L}$ achieves maximum, the step mainly influences the surface current. The step enlarges the length of current flow, and the influence of the step is equivalent to extending the length of the slit. The increment in the effective F–P cavity length can be expressed as δJ.

Actually, the step increases the effective length of the current flow and shortens the effective length of charge distribution at the same time. These two mechanisms take effect on the system simultaneously. For a small step as perturbation, we may ascribe the resonant wavelength as follows:

$$\lambda_{\rm res} = \frac{k_0 L_{\rm eff}}{N k_{\rm w}} = \frac{k_0}{N k_{\rm w}} \left(L_{\rm F-P} + \eta_{\rm L}\delta_{\rm J} - \eta_{\rm C}\delta_{\rm Q}\right), \tag{12}$$

where $L_{\rm eff}$ is the effective length of the slit with a step, $L_{\rm F-P}$ is the effective length of the bare slit, N is the mode number of the F–P cavity, and $k_{\rm w}$ (k_0) is the wave vector in the F–P cavity (in vacuum).

When the structure parameters h_2 and w_2 of the step are fixed, the values δJ and δQ are constants. As the step moves along the slit, the effective F–P cavity length $L_{\rm eff}$ is then determined by the relative coefficient of capacitance $\eta_{\rm C}$ and the relative coefficient of inductance $\eta_{\rm L}$. The $\eta_{\rm C}$ and $\eta_{\rm L}$ have a sinusoid-like function with the location h_3. From Eqs. (8) and (9), the phase difference between surface charge density σ and current density j at the same place in the slit is $\pi/2$, so the phase difference between $\eta_{\rm C}$ and $\eta_{\rm L}$ is also $\pi/2$, $\eta_{\rm C}$ and $\eta_{\rm L}$ alternately reach maximum with the change of h_3. As a result, the effective F–P cavity length $L_{\rm eff}$ oscillates with the location h_3 and hence the transmission peak oscillates with respect to the location h_3, which is proved by Fig. 3.

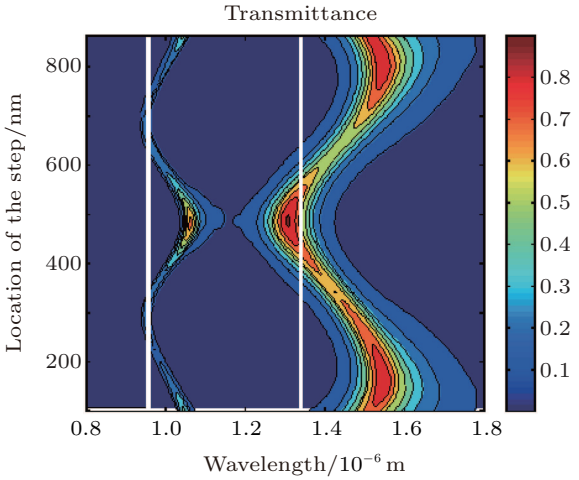


Fig. 3. (color online) Dependence of transmission spectra on the location of step h_3. Other parameters: the width w_2 is 270 nm, the length h_2 is 90 nm. The two white lines mark the resonant wavelength of the bare slit array.

Figure 4 presents the electromagnetic field of the slit with one step. Figure 4(a) describes the electric field in the slit for the first transmission peak in Fig. 3, figure 4(b) is the magnetic field for the first transmission peak, figure 4(c) is the electric field for the second transmission peak, figure 4(d) is the magnetic field for the second transmission peak. All other parameters are the same as in Fig. 3, and the step is in the middle of the slit $h_3 = 486$ nm. The step in the slit plays different roles for two transmission peaks. One decreases the effective length L_{eff}, as shown in Figs. 4(a) and 4(b). The other increases the effective length, as shown in Figs. 4(c) and 4(d). This fact proves our theory.

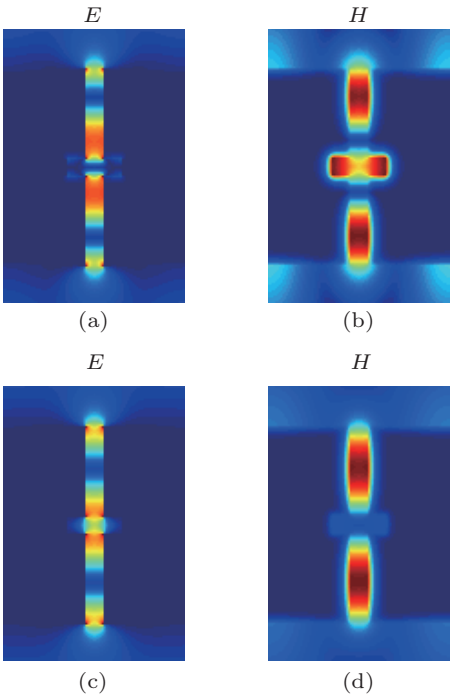


Fig. 4. (color online) The electric field (a) of the first transmission peak, the magnetic field (b) of the first transmission peak, the electric field (c) of the second transmission peak, the magnetic field (d) of the second transmission peak. All other parameters are the same as Fig. 3, and the step is in the middle of the slit $h_3 = 486$ nm.

The dependence of the transmission on the step length h_2 is described in Fig. 5. The step is located in the middle of the slit in the z-axis direction, and other parameters are the same as above. The step is located at the high magnetic field for the first transmission peak, and the step is located at the high electric field for the second one. To distinguish these two transmission peaks, the first transmission peak and the second transmission peak are named as the magnetic transmission peak and the electric transmission peak, respectively.

For the magnetic transmission peak (the first transmission peak in Fig. 5), the relative inductance coefficient η_{L} increases with the step length h_2 increasing, the relative capacitance coefficient η_{C} nearly approaches zero, the shortening length of the current flow δJ does not change with h_2 and the shortening length of δQ enlarges. From Eq. (12), the resonant wavelength λ_{res} is mainly decided by the relative inductance coefficient η_{L}, η_{L} behaves like a sinusoidal function with h_2 increasing, so the transmission wavelength behaves also sinusoidally with h_2 increasing. For the electric transmission peak (the second transmission peak in Fig. 5), the relative capacitance coefficient η_{C} increases, the relative inductance coefficient η_{L} approaches zero, the shortening length of the current flow δJ is unchanged, and the shortening length δQ linearly enlarges with h_2 increasing. From Eq. (12), the resonant wavelength λ_{res} is mainly decided by the product of η_{C} and δQ, λ_{res} mainly behaves as a sinusoid incline with h_2 increasing. The phase difference between the two transmission peaks also proving the phase difference $\pi/2$ between the η_{C} and η_{L}.

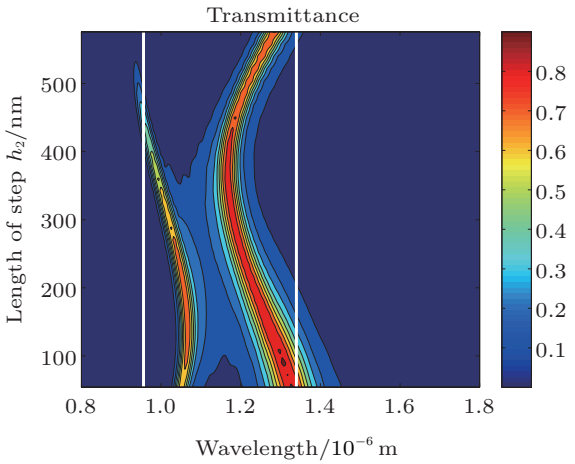


Fig. 5. (color online) Dependence of transmission spectra on the length of step h_2. Other parameters are $h_3 = 486$ nm, and $w_2 = 270$ nm. Two vertical dashed lines mark the resonant wavelength of the bare slit array.

The dependence of transmission on the step width w_2 is shown in Fig. 6. The step location is also fixed in the middle of the slit. Other parameters are the same as they are in Fig. 3. With the increase of the step width w_2, the lengthening of current flow δJ enlarges, and δQ almost does not change. From Eqs. (10) and (11), the relative inductance coefficient η_{L} and the relative capacitance coefficient η_{C} are fixed when w_2 changes. For the magnetic transmission peak (the first transmission peaks in Fig. 6), η_{L} keeps a large value, but η_{C} keeps a small value. The resonant wavelength λ_{res} is mainly decided by δJ, as predicted by Eq. (12). The transmission wavelength increases nearly linearly with w_2 increasing, which is shown as the first transmission peaks in Fig. 6. On the other hand, for the electric transmission peak (the second transmission peak in Fig. 6), η_{C} keeps a large value while η_{L} keeps a small value, λ_{res} is mainly decided by δQ. Because of the unchanged value of δQ, the transmission wavelength almost does not change with the length w_2, which is shown as the second transmission peak in Fig. 6. With w_2 increasing, these two peaks would unite to a peak.

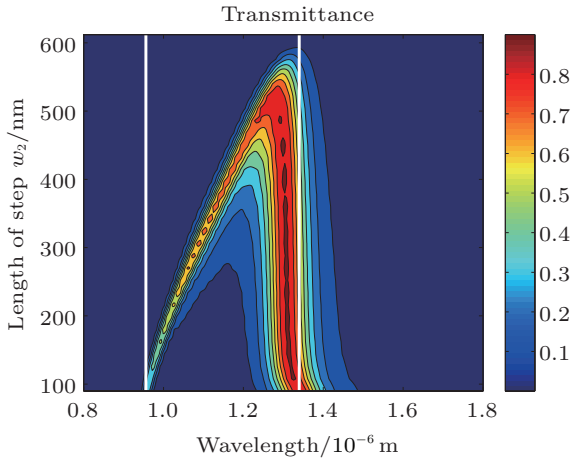


Fig. 6. (color online) Dependence of transmission spectra on the width w_2. Other parameters are $h_3 = 486$ nm, and $h_2 = 90$ nm. Two vertical dashed lines mark the resonant wavelength of the bare slit array.

From the above analysis, all parameters of the step can affect transmission wavelength through influencing effective F–P cavity length L_{eff}. From Eq. (12), the resonant wavelength λ_{res} is related with four coefficients. The location of the step h_3 only affects the relative inductance coefficient η_{L} and relative capacitance coefficient η_{C}, and does not affect effective length δJ and δQ. The step length h_2 affects η_{L}, η_{C}, and δQ, but does not influence δJ. The step width w_2 only affects δJ, and does not influence the other three coefficients.

3.3. Interaction of the multiple steps

If there are multi-steps in the slit, the effective length of the slit with multi-steps L_{eff} will be decided by this equation

$$L_{\text{eff}} = L_{\text{F-P}} + \sum \Delta L_i + \frac{1}{2}\sum I_{ij}, \tag{13}$$

where the $L_{\text{F-P}}$ is the effective length of the bare slit, ΔL_i is the influence of the i-th step, and I_{ij} is the interaction between the i-th step and the j-th step.

The interaction of multi-steps is hardly calculable when the number of steps is large. However, the standing wave in the slit can be considered as a circuit diagram in Fig. 2(f), so the effective length L_{eff} can be calculated by multiple adding of the influence of each single step.

To testify this theory, we explore the transmission spectra of the slit with two steps. One of these steps is fixed whose parameters do not change in the simulation. The parameters of the other are changed to testify the interaction between the multi-steps. The parameters of the fixed one are $h_{\text{f3}} = 648$ nm, $w_{\text{f2}} = 270$ nm, and $h_{\text{f2}} = 90$ nm. Other parameters are the same as they are in Fig. 2.

Figure 7 shows the dependence of the transmission spectra on the location of the changed step h_{c3}, the width w_{c2} is 270 nm, the length h_{c2} is 90 nm. Two white lines mark the resonant wavelength of the slit with a fixed step. The mode number is $N = 3$ for $\lambda = 956$ nm and $N = 2$ for $\lambda = 1446$ nm. For the changed step, η_{C} and η_{L} alternately reach the maximum with the change of h_{c3}. As a result, the effective length L_{eff} oscillates with location h_{c3} and hence the transmission peak oscillates with respect to location h_{c3}. The behaviors of these two transmission peaks are the same as they are in Fig. 3. The edge to edge distance between the changed and fixed steps is more than 36 nm. At this distance, there is not obvious coupling between the two steps, which can prove that the influence of adding the second step is the same as that of adding a single step.

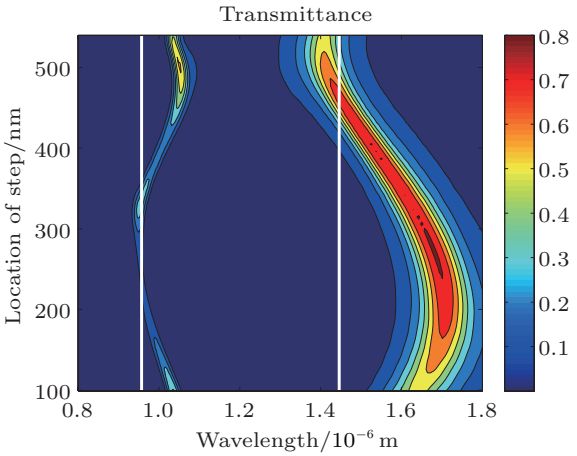


Fig. 7. (color online) Dependence of transmission spectra of two slits on the location of one change step h_{c3}. Other parameters: the width w_{c2} is 270 nm, the length h_{c2} is 90 nm. The parameters of the fixed step are $h_{\text{f3}} = 648$ nm, $w_{\text{f2}} = 270$ nm, and $h_{\text{f2}} = 90$ nm. The two white lines mark the resonant wavelength of a slit with a fixed step array.

The dependence of the transmission spectra on the length of the changed step h_{c2} is shown in Fig. 8. The width w_{c2} is 270 nm. For leaving enough interspace to vary the length of the changing step, the location h_{c3} is chosen at 324 nm. Other parameters are the same as they are in Fig. 7. Like figure 5, the two transmission peaks are also sinusoidal with h_{c2} increasing. It is mainly owned to the resonant absorbance that the first transmission peak disappears in the middle of the figure.

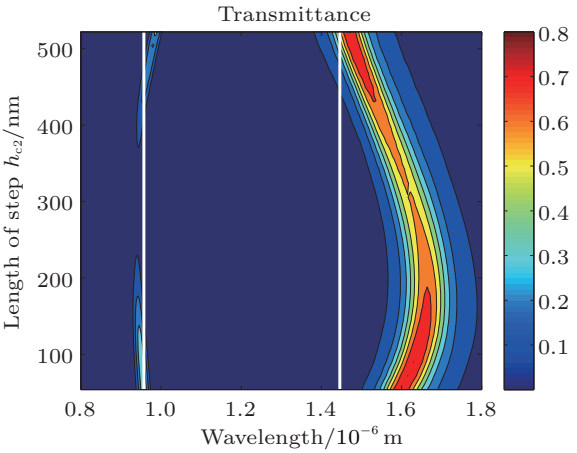


Fig. 8. (color online) Dependence of transmission spectra of two slits on the length of change step h_{c2}. Other parameters: the width w_{c2} is 270 nm, the location h_{c3} is 324 nm. The parameters of the fixed step are $h_{\text{f3}} = 648$ nm, $w_{\text{f2}} = 270$ nm, and $h_{\text{f2}} = 90$ nm. The two white lines mark the resonant wavelength of a slit with a fixed step array.

The dependence of the transmission spectra on the width w_{c2} is shown in Fig. 9. The location h_{c3} is 486 nm, the length h_{c2} is 90 nm. Other parameters are the same as they are in Fig. 7. Like figure 6, the first transmission peak in Fig. 9 increases nearly linearly with the w_{c2} increasing; the second transmission peak almost does not change with the length w_{c2}.

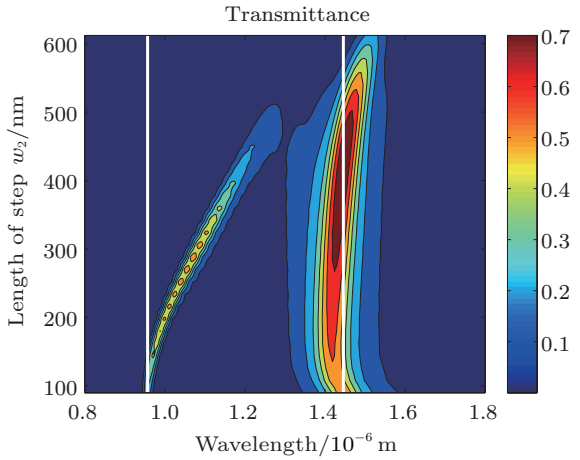


Fig. 9. (color online) Dependence of transmission spectra of two slits on the width w_{c2}. Other parameters: the location h_{c3} is 486 nm, the length h_{c2} is 90 nm. The parameters of the fixed step are $h_{f3} = 648$ nm, $w_{f2} = 270$ nm, and $h_{f2} = 90$ nm. The two white lines mark the resonant wavelength of a slit with a fixed step array.

All of above simulations prove that the effect of the second step in a slit with one step is the same as that of adding a step to a bare slit. Therefore, this method can be used to analyze the transmission of the multi-step in the slit.

3.4. Transmission of the fractal structure

Additionally, we explore the transmission spectra of a zero-three level 1/3 fractal structure fabricated in the slit. This structure is obtained through perforating steps on two walls of the slit, whose length is equal to 1/3 length of the previous level structure.

For slits with zero-level fractal steps, the parameters are chosen as $p = 900$ nm, $h_1 = 972$ nm, and $w_1 = 90$ nm. Two resonant wavelengths (956 nm and 1340 nm) appear in the investigated wavelength range. Obviously, the slit acts as F–P cavities according to Ref. [31], and the mode number is $N = 3$ for $\lambda = 956$ nm and $N = 2$ for $\lambda = 1340$ nm. Figure 10(a) presents the transmission spectrum of the bare slit.

Figure 10(b) describes the transmission of the slit with one-level fractal steps. The structure has only one step in the middle of the slit. This level fractal structure's parameters are listed as: The width of the additional step is three times the width of slit $w_{s1} = 3w_1 = 270$ nm, the length of the step is one third of the length of slit $h_{s1} = h_1/3 = 324$ nm. The location of the step is in the middle of slit $l_{s1} = 486$ nm. The other parameters are the same as that of the zero-level fractal structure. The schematic of a unit cell is shown in the inset of Fig. 10(b). For the transmission peak with mode number $N = 3$ (the first transmission peak in Fig. 10(b)), the one-level fractured structure is located at the antinode of the magnetic field, and thus the relative inductance coefficient η_L achieves maximum. From the above analysis, this transmission peak is the magnetic transmission peak, and the resonant wavelength slightly moves to long-wavelength direction under the influence of one-level fractal structure. For the transmission peak with mode number $N = 2$ (the second transmission peak in Fig. 10(b)), the structure is located at the antinode of the electric field, the relative capacitance coefficient η_C achieves maximum.

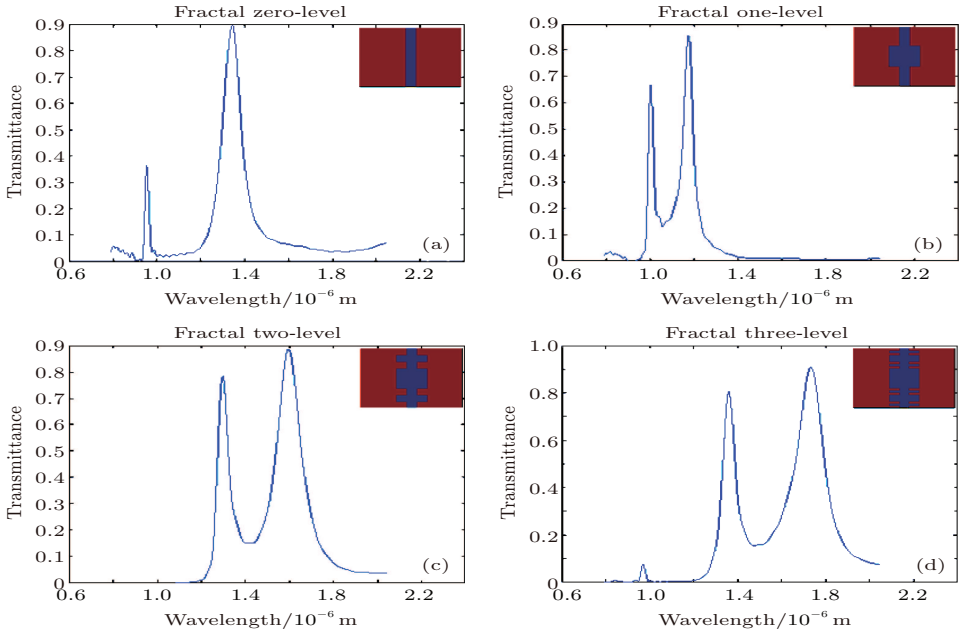


Fig. 10. (color online) Transmission spectra of the slit with fractal steps for different fractal levels. (a) Zero-level; (b) one-level; (c) two-level; (d) three-level.

The relative capacitance coefficient η_C achieves maximum. This transmission peak is the electric transmission peak, and the resonant wavelength moves to the short-wavelength direction due to the influence of structure.

Figure 10(c) is the transmission spectrum of the slit with two-level fractal steps. The two-level fractal structure is gained through adding another two steps to the previous structure. The additional steps have the same width as the one-level structure $w_{s2} = 270$ nm. The length of the adding step is one third of the one-level structure $h_{s2} = h_{s1}/3 = 108$ nm. The location of step is in the middle of the bare slit parts $l_{s2} = 243$ nm, and 729 nm. The other parameters are the same as that of the one-level fractal structure. The schematic of its unit cell is shown in the inset of Fig. 10(c). The two-level fractal steps are located at the antinode of the magnetic field for the two transmission peaks. The relative inductance coefficient η_L increases compared with the one-level fractal structure. From the above analysis, both transmission peaks move in the long-wavelength direction under the influence of the two-level fractal structure.

Figure 10(d) gives the transmission spectrum of the slit with a three-level fractal structure. Four steps are added to the two-level structure fractal structure to form the three-level fractal structure. The three-level additional steps have the same width as that of the previous level structures $w_{s3} =$ 270 nm. The length of the additional step is one third of the two-level structure $h_{s3} = h_{s2}/3 = 36$ nm. The location of the step is in the middle of the bare slit parts $l_{s3} = 121.5$ nm, 364.5 nm, 607.5 nm, and 850.5 nm. Other parameters are the same as that of the two-level fraction structure. The schematic of the unit cell is shown in the insert of Fig. 10(d). For two transmission peaks, two of the three-level fractal structures are located at the antinode of magnetic field, the other two steps are located at the antinode of the electric field, respectively. The change in the relative inductance coefficient η_L will be counteracted by the change in η_C. Therefore, these transmission peaks do not move obviously, compared with the peaks for two-level fractal structure. Compared with the previous situation, as the adding steps become more and more, the effective F–P cavity length L_{eff} of this complex structure increases. Therefore, a new transmission peak for mode number $N = 4$ appears in the transmission spectrum.

4. Summary

In summary, the transmission spectra of a normally incident plane wave through the sub-wavelength metallic slits curved with a single step or multi-steps are theoretically investigated. The influences of the SPP make the end of the finitely long sub-wavelength metallic slit behave as a magnetic-reflecting barrier. Because of the magnetic-reflecting barrier, the electromagnetic field in the slit is mainly a standing wave. The standing electromagnetic oscillation behaves like an LC oscillating circuit to select the frequency. The parameters of the step may change the transmission wavelength. Compared with previous research works, two new effective coefficients are introduced to explain the change of resonant wavelength. The parameters of the additional step that influence four effective coefficients on the transmission wavelength are discussed in detail. The influences of multi-adding steps is presented to analyze the interaction of two steps in the slit with multi-step. Finally, this theoretical model is verified through investigating the sub-wavelength metallic slits curved with a fractal structure. The proposed model can explain all the calculated results well.

References

[1] Ebbesen T W, Lezec H J, Ghaemi H F, Thio T and Wolff P A 1998 *Nature* **391** 667
[2] Lezec H J, Degiron A, Devaux E, Linke R A, Martin-Moreno L, Garcia-Vidal F J and Ebbesen T W 2002 *Science* **297** 820
[3] Barnes W L, Dereux A and Ebbesen T W 2003 *Nature* **424** 824
[4] Matsui T, Agrawal A, Nahata A and Vardeny Z V 2007 *Nature* **446** 517
[5] Genet C and Ebbesen T W 2007 *Nature* **445** 39
[6] Dintinger J, Klein S, Bustos F, Barnes W L and Ebbesen T W 2005 *Phys. Rev. B* **71** 035424
[7] Barnes W L, Murray W A, Dintinger J, Devaux E and Ebbesen T W 2004 *Phys. Rev. Lett.* **92** 107401
[8] Miyamaru F and Hangyo M 2005 *Phys. Rev. B* **71** 165408
[9] Qu D X and Grischkowsky D 2004 *Phys. Rev. Lett.* **93** 196804
[10] Rivas J G, Schotsch C, Bolivar P H and Kurz H 2003 *Phys. Rev. B* **68** 201306
[11] Astilean S, Lalanne P and Palamaru M 2000 *Opt. Commun.* **175** 265
[12] Takakura Y 2001 *Phys. Rev. Lett.* **86** 5601
[13] Cao Q and Lalanne P 2002 *Phys. Rev. Lett.* **88** 057403
[14] Lalanne P, Sauvan C, Hugonin J P, Rodier J C and Chavel P 2003 *Phys. Rev. B* **68** 125404
[15] Lee K G and Park Q H 2005 *Phys. Rev. Lett.* **95** 103902
[16] Tsai M W, Chuang T H, Meng C Y, Chang Y T and Lee S C 2006 *Appl. Phys. Lett.* **88** 071114
[17] Suckling J R, Hibbins A P, Lockyear M J, Preist T W and Sambles J R 2004 *Phys. Rev. Lett.* **92** 147401
[18] Xie Y, Zakharian A, Moloney J and Mansuripur M 2005 *Opt. Express* **13** 4485
[19] Cheng C, Chen J, Wu Q Y, Ren F F, Xu J, Fan Y X and Wang H T 2007 *Appl. Phys. Lett.* **91** 111111
[20] Ginzburg P and Orenstein M 2007 *Opt. Express* **15** 6762
[21] Shi H F, Wang C T, Du C L, Luo X G, Dong X C and Gao H T 2005 *Opt. Express* **13** 6815
[22] Shao D B and Chen S C 2005 *Appl. Phys. Lett.* **86** 253107
[23] Sun Z and Kim H K 2004 *Appl. Phys. Lett.* **85** 642
[24] Lockyear M J, Hibbins A P and Sambles J R 2007 *Appl. Phys. Lett.* **91** 251106
[25] Wang Y H, Wang Y Q, Zhang Y and Liu S T 2009 *Opt. Express* **17** 5014
[26] Wang Y Q, Wang Y H, Ye J S, Zhang Y and Liu S T 2011 *Opt. Commun.* **284** 877
[27] Ge D B and Yan Y B 2003 *Electromagnetic Algorithm: The Finite-Difference Time-Domain method* (Beijing: Electronic Science and Technology University Press)
[28] Taflove A and Hagness S C 2005 *Computational Electrodynamics: The Finite-Difference Time-Domain Method* (3rd edn.) (Boston: Artech House)
[29] Baida F I and Labeke D V 2003 *Phys. Rev. B* **67** 155314
[30] Gray S K and Kupka T 2003 *Phys. Rev. B* **68** 045415
[31] Shao D B and Chen S C 2005 *Opt. Express* **13** 6964
[32] Hibbins A P, Lockyear M J and Sambles J R 2006 *J. Appl. Phys.* **99** 124903
[33] Liu H T and Lalanne P 2008 *Nature* **452** 728